Acta Crystallographica Section D
Biological Crystallography
ISSN 0907-4449

Purification, crystallization, X-ray diffraction analysis and phasing of a Fab fragment of monoclonal neuroantibody αD11 against nerve growth factor

Sonia Covaceuszach,[a,b]* Alberto Cassetta,[c] Antonino Cattaneo[a,b] and Doriano Lamba[c,d]

[a]LayLineGenomics SpA, Via di Castel Romano 100, I-00128 Roma, Italy, [b]Neuroscience Program, International School for Advanced Studies, Via Beirut 2/4, I-34014 Trieste, Italy, [c]Istituto di Cristallografia, Consiglio Nazionale delle Ricerche, Unità Staccata di Trieste, Area Science Park – Basovizza, SS 14 Km 163.5, I-34012 Trieste, Italy, and [d]International Centre for Genetic Engineering and Biotechnology, Area Science Park, Padriciano 99, I-34012 Trieste, Italy

Correspondence e-mail: covaceu@sissa.it

Received 6 April 2004
Accepted 11 May 2004

The rat monoclonal neuroantibody αD11 is a potent antagonist that prevents the binding of nerve growth factor (NGF) to its tyrosine kinase A receptor (TrkA) in a variety of systems, most notably in two *in vivo* systems linked to crucial pathological states, such as Alzheimer's disease and HIV infection. To provide further insights into the mechanism of action of this potentially therapeutic monoclonal antibody, structural studies of the antigen-binding fragment (Fab) of αD11 were performed. αD11 IgG2a immunoglobulin was obtained from hybridomas by *in vitro* tissue culture. The αD11 Fab crystallizes in two crystal forms. Form I belongs to space group $P1$, with unit-cell parameters a = 42.7, b = 50.6, c = 102.7 Å, α = 82.0, β = 89.1, γ = 86.0°. With two molecules in the asymmetric unit, V_M is 2.3 Å^3 Da^{-1} and the solvent content is 46%. A complete data set has been collected at 2.7 Å resolution on beamline XRD-1 (ELETTRA, Trieste, Italy). Form II belongs to space group $C2$, with unit-cell parameters a = 114.8, b = 69.4, c = 64.10 Å, β = 117.0°. With one molecule in the asymmetric unit, V_M is 2.4 Å^3 Da^{-1} and the solvent content is 48%. A complete data set has been collected at 1.7 Å resolution on beamline ID14-1 (ESRF, Grenoble, France). Phasing was successfully performed by Patterson search techniques and refinement of the structures is currently under way. Crystal forms I and II display a close-packing pattern.

1. Introduction

The rat monoclonal antibody αD11 is able to bind with high affinity with NGF, a member of the neurotrophin superfamily, and to neutralize its biological function. This key trophic factor is crucial in both the development and the maintenance of the specific neuronal population of the peripheral and central nervous system. αD11 distinctively recognizes the native form of the antigen and strongly abolishes the interaction towards its specific high-affinity receptor TrkA, which mediates NGF biological functions.

It is worthy of note that NGF–TrkA interaction is implicated in important disease states. In addition to potential therapeutic application of NGF agonists for the treatment of neurodegenerative diseases and nervous-system injuries (Cuello, 1996; Mufson *et al.*, 1997), NGF antagonists would also be useful in the treatment of certain chronic inflammatory or neuropathic pain states mediated by TrkA. Moreover, several human malignancies express normal TrkA and are NGF-dependent or NGF-responsive; among these are not only neuroectoderm-derived tumours, such as medulloblastomas (Revoltella & Butler, 1980; Bauer *et al.*, 1992), neuroblastomas and glioblastomas (Oelmann *et al.*, 1995), but also non-neuronal carcinomas (Koizumi *et al.*, 1998) such as melanomas (Marchetti *et al.*, 1996), medullary thyroid carcinomas (Goretzki *et al.*, 1987; McGregor *et al.*, 1999), pancreatic carcinoid cell lines (Bold *et al.*, 1995) and prostate (Djakiew *et al.*, 1991), breast (Tagliabue *et al.*, 2000) and lung carcinomas. In addition, NGF has been shown to be an autocrine factor that is essential for the survival of macrophages infected with human immunodeficiency virus, contributing to the maintainance of this crucial reservoir for HIV in the body (Garaci *et al.*, 1999; Balestra *et al.*, 2001; Harrold *et al.*, 2001).

αD11 is a monoclonal antibody of subclass IgG2a, generated against mouse NGF (Cattaneo *et al.*, 1988) after a long-term immunization of rats. This antibody has been cloned, sequenced and expressed (Ruberti *et al.*, 1993). It has been demonstrated that αD11 neutralizing activity *in vivo* is specific for NGF, with no cross-reactivity towards closely related members of the neurotrophin superfamily, and therefore this blocking antibody has been used extensively for *in vivo* experiments (Maffei *et al.*, 1992; Berardi *et al.*, 1994; Domenici *et al.*, 1994; Molnar *et al.*, 1997, 1998).

Most importantly, αD11 has been expressed in the nervous system of transgenic mice (Ruberti *et al.*, 2000) by the neuroantibody technique (Cattaneo & Neuberger, 1987;

Cattaneo *et al.*, 1988; Piccioli *et al.*, 1995). Considering that effective inhibition of NGF actions occurs in adult animals only, anti-NGF mice provided a unique opportunity to study the consequences of a chronic deprivation of NGF in aged animals. The observed phenotype (Capsoni *et al.*, 2000) closely resembled that found in Alzheimer's disease (AD; Selkoe, 1991; Goedert, 1998), displaying a full complement of phenotypic hallmarks of the disease and therefore representing a comprehensive transgenic model for AD.

Moreover, in a recent study that used severe combined immunodeficient mice engrafted with human peripheral blood lymphocytes to investigate the *in vivo* effect of HIV-1-infected macrophages on virus spread and CD4+ T-lymphocyte depletion, the αD11 monoclonal antibody was able to suppress *in vivo* the pathogenetic events mediated by infected macrophages (Garaci *et al.*, 2003).

The overall aim of our studies is to characterize the interaction between αD11 and its antigen. Although several monoclonal antibodies have been raised against NGF, αD11 deserves special interest since it has been shown to interfere *in vivo* with high affinity with the function of NGF. The lack of cross-reactivity with other members of the neurotrophin family strongly suggests that the residues present in non-analogous regions of NGF and that are responsible for the receptor specificity may be involved in antibody recognition. The present structural investigation, along with the crystallographic analysis of the second immunoglobulin-like domain d5 of TrkA bound to NGF (Wiesmann *et al.*, 1999), should provide important insights for understanding the molecular basis of antibody specificity for the NGF antigen and its mode of interaction with the full-length receptor.

Furthermore, detailed structural information on antigenic recognition by αD11 is expected to aid in the development of analogues as antagonists or agonists of neurotrophins, which may have greater affinity or specificity for further experimental and therapeutic applications in many pathological contexts. As a first step towards the comprehension of TrkA–NGF binding and recognition mechanisms, we report the purification, crystallization and preliminary X-ray analysis of the αD11 Fab.

(*a*)

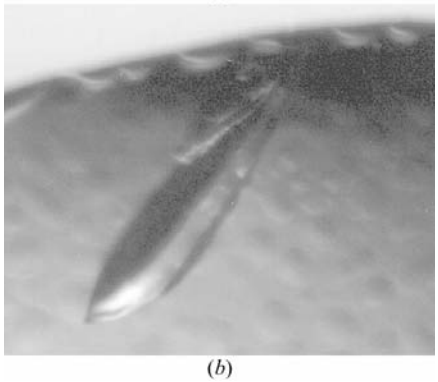

(*b*)

Figure 1
αD11 Fab crystals: (*a*) form I (∼0.2 × 0.1 × 0.1 mm in size), (*b*) form II (∼0.7 × 0.4 × 0.2 mm in size).

2. Experimental and results

2.1. Purification of the αD11 Fab

The αD11 hybridoma was prepared according to Cattaneo *et al.* (1988). The αD11 IgG2a immunoglobulin was purified from hybridoma supernatant by precipitation with 29% ammonium sulfate followed by affinity chromatography using a Protein G Sepharose column (Pharmacia) and was eluted with low-pH buffer (10 m*M* HCl). αD11 IgG2a fractions were pooled and dialyzed across a Spectra-Por 12/14K membrane (Spectrum) against 10 m*M* sodium phosphate pH 7.0 and 20 m*M* EDTA. The αD11 IgG2a protein solution (10 mg ml^{-1}) was incubated with 13 m*M* Cys and treated with immobilized papain (Pierce; at an enzyme:substrate ratio of 1:15) for 5 h at 310 K. The resulting digest was dialyzed overnight against 10 m*M* sodium phosphate pH 7.8. The removal of Fc fragments was achieved by passage through a DEAE-Sephacel (Pharmacia) column equilibrated with the same buffer. The αD11 Fab was collected in the flowthrough, while Fc fragments and a fraction of uncleaved IgG2a were eluted by 200 m*M* sodium phosphate pH 6.8. The Fab fragment was separated from the uncleaved IgG2a by size-exclusion chromatography on a Superdex G75 column (Pharmacia) equilibrated with 10 m*M* sodium phosphate pH 7.8 and 150 m*M* NaCl. Fractions were assessed for homogeneity by Coomassie blue staining after separation by SDS–PAGE. The amounts of purified protein were determined by Lowry assay (Bio-Rad).

2.2. Crystallization

The purified αD11 Fab fragment in 10 m*M* sodium phosphate pH 7.8 and 50 m*M* NaCl was concentrated to 5–10 mg ml^{-1} using Centricon 30K concentrators (Amicon). Initial crystallization experiments were based on the sparse-matrix sampling method (Jancarik & Kim, 1991) using Crystal Screens I and II (Hampton Research, CA, USA) and the Jena BioSciences sparse-matrix crystallization screening kits. Preliminary crystallization conditions were established using the hanging-drop vapour-diffusion method at 289 K. The most promising results were obtained from 20% PEG 4000, 0.6 *M* NaCl and 100 m*M* MES pH 6.5 (Jena BioSciences kit No. 4, solution C2). Unfortunately, analysis of the diffraction patterns of several crystals revealed that these were not single crystals and therefore not suitable for data collection, despite diffracting to 2.0 Å resolution on the XRD-1 beamline at ELETTRA (Trieste, Italy) .

These crystals could be partially optimized by lowering the pH and exchanging the precipitant buffer to 100 m*M* 1,3-bis-[tris(hydroxymethyl)methylamino]propane (BTP) pH 5.5. Under these conditions, crystals grew at a slower rate and reached a suitable size over a period of several months; single crystals, denominated crystal form I, are shown in Fig. 1(*a*). However, they only diffracted to 2.7 Å resolution.

Diffraction-quality crystals eventually grew under optimized conditions [20%(*w*/*v*) PEG 4000, 0.6 *M* NaCl, 100 m*M* BTP pH 5.5] and with a protein:precipitant volume ratio of 1.5. Crystals reached maximum dimensions over a period of several weeks. A typical Fab αD11 crystal, denominated crystal form II, is shown in Fig. 1(*b*).

2.3. Data collection

Complete data sets were collected from crystal form I (0.3 × 0.2 × 0.1 mm) to 2.7 Å resolution using a MAR CCD detector (MAR USA Inc., USA) on the XRD-1 beamline at ELETTRA (Trieste, Italy) and from crystal form II (0.7 × 0.4 × 0.2 mm) to 1.7 Å resolution on the ID14-EH1 beamline at the ESRF (Grenoble, France). Both crystals were directly flash-cooled in a liquid-nitrogen stream at 100 K using an Oxford Cryosystems cooling device (Oxford Cryosystems Ltd., England), with no need for transfer to a cryoprotectant solution. X-ray diffraction data were indexed, integrated and subsequently scaled using the programs *DENZO* and *SCALEPACK* (Otwinowski & Minor, 1997), respectively,

Table 1
Crystal parameters, data-collection and processing statistics.

Values in parentheses are for the highest resolution shell.

Crystal	Form I	Form II
X-ray source	ELETTRA	ESRF
Wavelength (Å)	1.000	0.934
Detector	MAR CCD	MAR CCD
Space group	*P*1	*C*2
Unit-cell parameters		
a (Å)	42.68	114.80
b (Å)	50.63	69.35
c (Å)	102.70	64.10
α (°)	81.98	90
β (°)	89.12	117.02
γ (°)	85.96	90
Z	2	4
Mosaicity (°)	0.44	0.40
Resolution range (Å)	47.6–2.7 (2.8–2.7)	17.0–1.70 (1.75–1.70)
No. measurements	159467	492593
No. observed reflections, $I \geq 0$	101370	300662
No. unique reflections, $I \geq 0$	23413 (2162)	47951 (3198)
Completeness (%)	98.2 (92.4)	97.2 (78.4)
Redundancy	4.3 (4.0)	6.1 (3.7)
$\langle I/\sigma(I)\rangle$ of measured data	11.5 (5.4)	5.8 (5.5)
$R_{\rm sym}$† (%)	11.0 (33.5)	5.8 (27.8)

† $R_{\rm sym}(I) = \sum_{hkl}\sum_i |I_{hkl,i} - \langle I_{hkl}\rangle|/\sum_{hkl}\sum_i |I_{hkl,i}|$, where $\langle I_{hkl}\rangle$ is the mean intensity of the multiple $I_{hkl,i}$ observations from symmetry-related reflections.

and the *CCP*4 package (Collaborative Computational Project, Number 4, 1994) was used for data reduction. Surprisingly, although the crystallization conditions only differed in the protein:precipitant ratio, the two crystals belong to the triclinic *P*1 (form I) and monoclinic *C*2 (form II) space groups, respectively. The data-collection statistics are summarized in Table 1. Assuming a molecular weight of 48 100 Da and two molecules in the asymmetric unit for crystal form I, the crystal-packing parameter $V_{\rm M}$ is 2.28 Å^3 Da^{-1}, corresponding to a solvent content of 46.0%. Assuming one molecule in the asymmetric unit, $V_{\rm M}$ is 2.36 Å^3 Da^{-1} for crystal form II, corresponding to a solvent content of 47.9% (Matthews, 1968).

2.4. Phasing

Given that a number of crystal structures of Fab fragments are available, the most appropriate technique for the determination of the αD11 Fab structure is a Patterson search. Following a close scrutiny of the structures in the Protein Data Bank (Berman *et al.*, 2000), 1cic, the structure of an idiotope–anti-idiotope complex FabD1.3–FabE225 (Bentley *et al.*, 1990), was chosen as search model (FabD1.3). This structure appeared to be the most suitable on the basis of resolution (2.5 Å) and sequence identity (81.95 and 82.65% for the heavy and light variable domains, respectively). The length of the CDRs matches the loop length in the αD11 Fab with the unique exception of the αD11_CDRH3 Fab, which is six residues longer.

Table 2
Molecular replacement (all calculations were carried out with data in the 15.0–3.5 Å resolution range).

Results for variable-domain and constant-domain searches with the rotation function ($R_{\rm v}$ and $R_{\rm c}$, respectively) and the single-body translation function ($T_{\rm v}$ and $T_{\rm c}$, respectively) are shown as the peak height of the correct solution and the largest noise peak (given in parentheses). The peak heights correspond to the correlation coefficient as a percentage.

Crystal	Form I	Form II
$R_{\rm v}$	21.3 19.2 (13.3)	19.9 (7.9)
$R_{\rm c}$	17.9 14.7 (11.8)	12.3 (6.4)
$T_{\rm v}$	21.3 33.8	29.1 (18.9)
$T_{\rm c}$	42.5 46.5 (39.5)	18.4 (13.2)
Rigid-body refinement		
R factor (%)	39.8	38.9
Correlation coefficient	54.8	49.7

A molecular-replacement solution for the αD11 Fab was obtained using *AMoRe* (Navaza, 1994) on the low-resolution data set collected for crystal form I. It is well known that the so-called elbow angle of Fab molecules varies considerably between different crystal structures. Therefore, the search model was divided into variable and constant domains; the variable domains included residues 1–109 of the light chain and 1–114 of the heavy chain, while the constant domains included the rest of the molecule (residues 110–214 of the light chain and 115–218 of the heavy chain). The rotation function gave clear indications of the orientation of the variable and constant domains for the two Fab fragments present in the asymmetric unit. These orientations were in turn used for the translation function, in which the correct solutions proved to be the highest peak in each case. A four-body translation function was then calculated in order to confirm the consistency of the independent solutions for the variable and constant domains and to place these four components on a common crystallographic origin. Rigid-body refinement was subsequently performed in order to optimize the orientation and position of the two Fab fragments related by a non-crystallographic pseudo-twofold axis. The packing of the structure was inspected visually. In order to carry out the crystallographic refinement using the high-resolution data set collected from crystal form II, a molecular-replacement search was again performed, now exploiting as the probe one of the two Fab fragments previously located in crystal form I, and subjected to a preliminary model building (mutation of non-homologous residues and deletion of less conserved CDRH3 or poorly defined loop regions). Since the elbow angle shows great variability, not only among different Fab fragments but also among different crystal forms of the same Fab fragment, molecular replacement was performed using the constant and variable domains as a search model separately. Details of the molecular-replacement results obtained for the two crystal forms are summarized in Table 2. The final models for both crystal forms have structurally sensible pairing of the heavy and light variable domains, with no steric hindrance to the packing of the Fab molecules, thus confirming the correctness of the solutions.

Current efforts are focused on model building and structure refinement using the high-resolution X-ray diffraction data set from crystal form II collected at ESRF (Grenoble, France).

2.5. Crystal packing

The αD11 Fab crystallized in two different space groups. However, the monoclinic *C*2 and the triclinic *P*1 crystal forms display similar packing patterns. The non-crystallographic pseudo-twofold axis (177°) that relates the two molecules in the triclinic cell probably corresponds to the crystallographic twofold axis in the monoclinic *C*2 space group. A stereo diagram of the crystal packing for crystal form II is shown in Fig. 2(*a*).

Edmundson *et al.* (1999) pointed out that general packing schemes in crystals of Fab fragments are determined by (i) the formation of hydrogen bonds across at least one twofold symmetry axis relating molecules within the unit cell (extended β-pleated sheets link two Ig domains in an antiparallel arrangement) and (ii) shape complementarity. Both types can occur independently or in concert in a crystal. Moreover, the former packing scheme frequently involves the constant domains of the heavy chains and/or one of the two classes of the light chains. In addition, for αD11 Fab, the main crystal contacts in forms I and II involve tail-to-tail interactions through the constant domain of the heavy chain to form cross-molecule extended β-pleated sheets (dimers). The contact region encompasses the conserved sequence in FabD1.3 (Bentley *et al.*, 1990), the structure of which was chosen as a search model for phasing,

i.e. SerH197-ThrH198-LysH199-ValH200-GluH201-LysH202-LysH203 (Fig. 2*b*). Two pairs of hydrogen bonds occur across the 3–3 β-strands; the backbone amides of AspH201 and LysH203 are engaged with the carbonyl groups of LysH199 and SerH197, respectively. Side chains emerge at right angles to the polypeptide chain and do not interfere with the intermolecular backbone interactions (Fig. 2*b*).

In αD11 Fab crystals, the formation of cross-molecule extended β-pleated sheets is necessary but not sufficient to produce a stable crystal lattice. Indeed, in Fab αD11 crystals a second type of interaction determined by shape complementarity occurs in concert with antiparallel stacking of constant domains. Such supplementary interactions have been described previously and can be as complicated as the insertion of exposed hydrophobic side chains of one molecule into the binding site of another (Edmundson *et al.*, 1974) or as simple as the steric fitting of knobs into holes (Faber *et al.*, 1998). Interestingly, the antigen-binding sites are partially involved in these secondary interactions; an analogy here is an antigen–antibody complex (blue arrow in Fig. 2*a*). Further additional contacts involve weak head-to-tail van der Waals interactions between the variable domain of the heavy chain and the constant domain of the light chain of a symmetry-related molecule (green arrow in Fig. 2*a*).

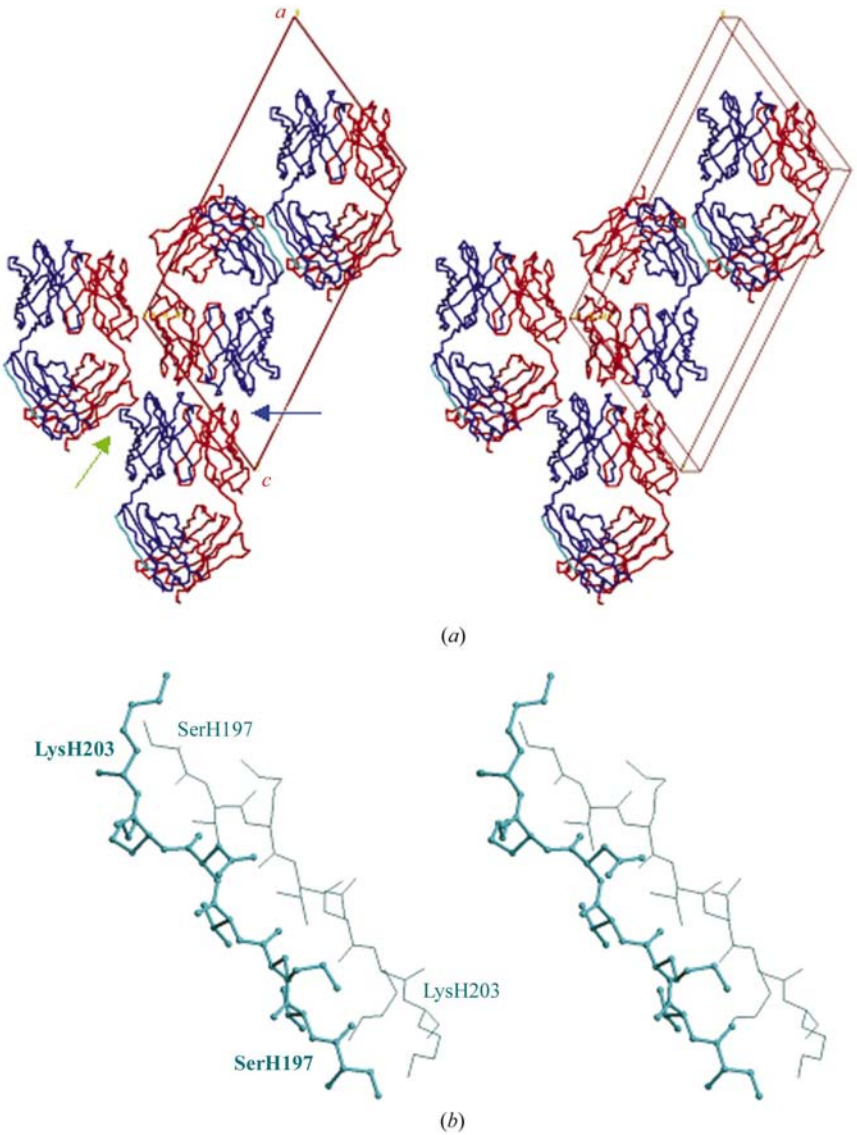

Figure 2
Crystal-packing analysis, using the search model, of the molecular-replacement solution for the αD11 Fab in crystal form II. (*a*) Stereoview along *b* of the packing contacts (light and heavy chains are coloured red and blue, respectively); the extended β-sheets linking the lateral β-strands of symmetry-related molecules are shown in cyan. Packing contacts led by shape complementarities engage the antigen-binding sites of symmetry-related molecules (blue arrow). Additional contacts (green arrow) involve molecules translated along *c*. (*b*) A closer stereoview, at the dimer interface, of the antiparallel β-strand encompassing SerH197-ThrH198-LysH199-ValH200-GluH201-LysH202-LysH203.

The authors thank the beamline scientists at ELETTRA (Trieste, Italy) and ESRF (Grenoble, France) for their excellent support and Gabriella Rossi for her skillful technical assistance.

References

Balestra, E., Perno, C. F., Aquaro, S., Panti, S., Bertoli, A., Piacentini, M., Forbici, F., D'Arrigo, R., Calio, R. & Garaci, E. (2001). *J. Biol. Regul. Homeost. Agents*, **15**, 272–276.
Bauer, J., Margolis, M., Schreiner, C., Edgell, C.-J., Azizkhan, J., Lazarowski, E. & Juliano, R. L. (1992). *J. Cell. Physiol.* **153**, 437–449.
Bentley, G. A., Boulot, G., Riottot, M. M. & Poljak, R. J. (1990). *Nature* (*London*), **348**, 254–257.
Berardi, N., Cellerino, A., Domenici, L., Fagiolini, M., Pizzorusso, T., Cattaneo, A. & Maffei, L. (1994). *Proc. Natl Acad. Sci. USA*, **91**, 684–688.
Berman, H. M., Westbrook, J., Feng, Z., Gilliland, G., Bhat, T. N., Weissig, H., Shindyalov, I. N. & Bourne, P. E. (2000). *Nucleic Acids Res.* **28**, 235–242.
Bold, R. J., Ishizuka, J., Rajaraman, S., Perez-Polo, R., Townsend, C. M. Jr & Thompson, J. C. (1995). *J. Neurochem.* **64**, 2622–2628.
Capsoni, S., Ugolini, G., Comparini, A., Ruberti, F., Berardi, N. & Cattaneo, A. (2000). *Proc. Natl Acad. Sci. USA*, **97**, 6826–6831.
Cattaneo, A. & Neuberger, M. S. (1987). *EMBO J.* **6**, 2753–2758.
Cattaneo, A., Rapposelli, B. & Calissano, P. (1988). *J. Neurochem.* **50**, 1003–1010.
Collaborative Computational Project, Number 4 (1994). *Acta Cryst.* D**50**, 760–763.
Cuello, A. C. (1996). *Prog. Brain Res.* **109**, 347–358.
Djakiew, D., Delsite, R., Pflug, B. R., Wrathall, J., Lynch, J. H. & Onoda, M. (1991). *Cancer Res.* **51**, 3304–3310.
Domenici, L., Cellerino, A., Berardi, N., Cattaneo, A. & Maffei, L. (1994). *Neuroreport*, **5**, 2041–2044.
Edmundson, A. B., De Witt, C. R., Goldsteen, B. Z. & Ramsland, P. A. (1999). *J. Cryst. Growth*, **196**, 276–284.
Edmundson, A. B., Ely, K. R., Girling, R. L., Abola, E. E., Schiffer, M. & Westholm, F. A. (1974). *Progress in Immunology II*, Vol. 1, edited by L. Brent & J. Holborow, p. 103. Amsterdam: North-Holland.
Faber, C., Shan, L., Fan, Z. C., Guddat, L. W., Furebring, C., Ohlin, M., Borrebaeck, C. A. K. & Edmundson, A. B. (1998). *Immunotechnology*, **3** 253–270.
Garaci, E., Aquaro, S., Lapenta, C., Amendola, A., Spada, M., Covaceuszach, S., Perno, C. F. & Belardelli, F. (2003). *Proc. Natl Acad. Sci. USA*, **100**, 8927–8932.
Garaci, E., Caroleo, M. C., Aloe, L., Aquaro, S., Piacentini, M., Costa, N., Amendola, A., Micera, A., Calio, R., Perno, C. F. & Levi-Montalcini, R. (1999). *Proc. Natl Acad. Sci. USA*, **96**, 14013–14018.
Goedert, M. (1998). *Prog. Brain Res.* **117**, 287–306.

Goretzki, P. E., Wahl, R. A., Becher, R., Koller, C., Branscheid, D., Grussendorf, M. & Roeher, H. D. (1987). *Surgery*, **102**, 1035–1042.
Harrold, S. M., Dragic, J. M., Brown, S. L. & Achim, C. L. (2001). *Adv. Exp. Med. Biol.* **493**, 41–47.
Jancarik, J. & Kim, S.-H. (1991). *J. Appl. Cryst.* **24**, 409–411.
Koizumi, H., Morita, M., Mikami, S., Shibayama, E. & Uchikoshi, T. (1998). *Pathol. Int.* **48**, 93–101.
McGregor, L. M., McCune, B. K., Graff, J. R., McDowell, P. R., Romans, K. E., Yancopoulos, G. D., Ball, D. W., Baylin, S. B. & Nelkin, B. D. (1999). *Proc. Natl Acad. Sci. USA*, **96**, 4540–4545.
Maffei, L., Berardi, N., Domenici, L., Parisi, V. & Pizzorusso, T. (1992). *J. Neurosci.* **12**, 4651–4662.
Marchetti, D., McQuillan, D. J., Spohn, W. C., Carson, D. D. & Nicolson, G. L. (1996). *Cancer Res.* **56**, 2856–2863.
Matthews, B. W. (1968). *J. Mol. Biol.* **33**, 491–497.
Molnar, M., Ruberti, F., Cozzari, C., Domenici, L. & Cattaneo, A. (1997). *Neuroreport*, **8**, 575–579.
Molnar, M., Tongiorgi, E., Avignone, E., Gonfloni, S., Ruberti, F., Domenici, L. & Cattaneo, A. (1998). *Eur. J. Neurosci.* **10**, 3127–3140.
Mufson, E. J., Lavine, N., Jaffar, S., Kordower, J. H., Quirion, R. & Saragovi, H. U. (1997). *Exp. Neurol.* **146**, 91–103.
Navaza, J. (1994). *Acta Cryst.* A**50**, 157–163.
Oelmann, E., Sreter, L., Schuller, I., Serve, H., Koenigsmann, M., Wiedenmann, B., Oberberg, D., Reufi, B., Thiel, E. & Berdel, W. E. (1995). *Cancer Res.* **55**, 2212–2219.
Otwinowski, Z. & Minor, W. (1997). *Methods Enzymol.* **276**, 307–326.
Piccioli, P., Di Luzio, A., Amann, R., Schuligoi, R., Azim Surani, M., Donnerer, J., Cattaneo, A. (1995). *Neuron*, **15**, 373–384.
Revoltella, R. P. & Butler, R. H. (1980). *J. Cell. Physiol.* **104**, 27–33.
Ruberti, F., Bradbury, A., Cattaneo, A. (1993). *Cell Mol Neurobiol.* **13**, 559–568.
Ruberti, F., Capsoni, S., Comparini, A., Di Daniel, E., Franzot, J., Gonfloni, S., Rossi, G., Berardi, N. & Cattaneo, A. (2000). *J. Neurosci.* **20**, 2589–2601.
Selkoe, D. J. (1991). *Neuron*, **6**, 487–498.
Tagliabue, E., Castiglioni, F., Ghirelli, C., Modugno, M., Asnaghi, L., Somenzi, G., Melani, C. & Menard, S. (2000). *J. Biol. Chem.* **275**, 5388–5394.
Wiesmann, C., Ultsch, M. H., Bass, S. H. & de Vos, A. M. (1999). *Nature* (*London*), **401**, 184–188.